Nanoscale

PAPER

View Article Online
View Journal | View Issue

Cite this: *Nanoscale*, 2026, **18**, 3067

Disentangling melanin self-assembly *via* nanoprecipitation: from protoparticles to supraparticles

Meera Madhu, Adithya Vaidyanathan, Bárbara Fornaciari and Bern Kohler *

The physicochemical properties of eumelanin, the dark melanin pigment found in most organisms, depend sensitively on the size and morphology of the particles that make up this naturally occurring nanomaterial. Past strategies for controlling nanostructure have focused on modulating the rate of the oxidation reactions that yield melanin from precursor compounds, making it difficult to decouple oxidative polymerization from self-assembly. Here, we introduce a post-synthetic approach that uses an organic antisolvent to isolate nanoscale assembly, aggregating ultrasmall, disc-like melanin particles that are 2–6 nm in diameter and contain only a few stacked layers of planar, sheet-like polycyclic molecules into size-controlled spherical supraparticles with diameters that can be tuned from 30 to 100 nm. Following dialysis to remove the organic solvent, the supraparticles are stable to heating and sonication and their size remains constant in water for at least two weeks. The excellent stability of the supraparticles is attributed to self-crosslinking reactions that form covalent bonds between the aggregated subunits. The bonds form slowly over hours by spontaneous reactions that can be accelerated by UV irradiation. The nanoprecipitation approach to creating melanin supraparticles offers a straightforward means to manipulate the hierarchical structure of melanin with the precision needed to enable investigations that can uncover melanin's emergent properties through structure–function studies.

Received 10th November 2025,
Accepted 9th January 2026

DOI: 10.1039/d5nr04738b

rsc.li/nanoscale

Introduction

Melanin is a family of ubiquitous biological pigments found across all kingdoms of life, including bacteria, fungi, plants, and animals. Melanins are biosynthesized by the oxidative polymerization of small aromatic molecule precursors with minimal intervention by enzymes.[1] Melanins serve multiple essential biological functions, such as UV protection, free radical scavenging, metal ion chelation, and redox buffering.[2] Beyond these natural roles, eumelanin, the brown-black melanin, and its synthetic analogues have garnered growing interest for their potential in bioelectronics, solar energy harvesting and storage, and a range of biomedical applications.[3,4] Unfortunately, the complex and spontaneous reactions that lead to melanin pigments are poorly understood, and the atomistic structures present in the final pigments are obscure despite a century of study.

In nature, melanin exhibits a rich variety of nano- and mesoscale structures that are critical to its diverse functions. In fungi, melanin is found as granules embedded in the cell wall, whereas in animals, it is predominantly confined within melanosomes—membrane-bound organelles whose shape and internal structure can vary widely (*e.g.*, spherical, rod-like, elongated, hollow, or flattened).[5] These hierarchical architectures are thought to emerge from the progressive assembly of eumelanin starting from small oligomeric units, which ultimately aggregate into nano- or micrometer-scale particles. A well-known example of nanostructure–function correlation is found in bird feathers, where the morphology and spatial arrangement of melanin nanostructures produce vivid structural coloration (iridescence).[6,7] An example in humans is the altered self-assembly behavior of eumelanin in melanoma cells, which suggests that changes in nanostructure may be associated with disease progression.[8]

Given the evidence that melanin's desirable properties (*i.e.*, optical absorption,[9,10] fluorescence,[10,11] free radical generation and scavenging behaviors[9,12]) are strongly influenced by its degree of aggregation and nanostructure, there is great interest in controlling these characteristics in so-called synthetic melanins made in the laboratory. However, the ability to do so is currently rudimentary and does not approach nature's exquisite level of control. Synthetic parameters such as the choice of precursor,[13] precursor concentration,[14,15] temperature,[14,15] oxidant type and concentration,[14–16] photoirradiation,[17] and

Department of Chemistry and Biochemistry, The Ohio State University, 100 West 18th Avenue, Columbus, Ohio 43210, USA. E-mail: kohler@chemistry.ohio-state.edu

the presence of agents that scavenge or generate radicals[18] have all been shown to influence particle size and morphology when synthetic eumelanin nanoparticles are made from precursors like dopamine and L-dihydroxyphenylalanine (L-DOPA), yielding dopamine melanin (also known as polydopamine, PDA) and DOPA melanin (DOPAm), respectively. However, in these approaches the covalent bond forming reactions that join precursor molecules into larger covalent structures occur concurrently with self-assembly (Fig. 1a), preventing the separate control of each.

Given the richness of the hierarchical structures found in natural melanins, we hypothesize that precursor polymerization and subunit aggregation may not be as temporally entangled during biosynthesis as when synthetic melanins are made in the lab. To test this concept, we focus in this study on achieving control over the aggregation of pre-synthesized synthetic melanin subunits (Fig. 1b). The concept that nanoparticles can be built from smaller nanoparticles has been used extensively to fabricate crystalline supraparticles and superlattices from inorganic particles using techniques such as solvent evaporation,[19,20] emulsion-templated assembly,[21] and electrostatic coassembly.[22,23] Supraparticles are hierarchical structures made through the ordered assembly of smaller particles. Recently, supra-carbon dots, which are self-assembled structures of carbon dots, have attracted attention for their tunable optical properties, enhanced photocatalytic activity, and potential in biomedical applications.[24] In the case of melanin, supraparticles tens of micrometers in diameter have been assembled from synthetic melanin nanoparticles encapsulated in a silica shell using a reverse emulsion method

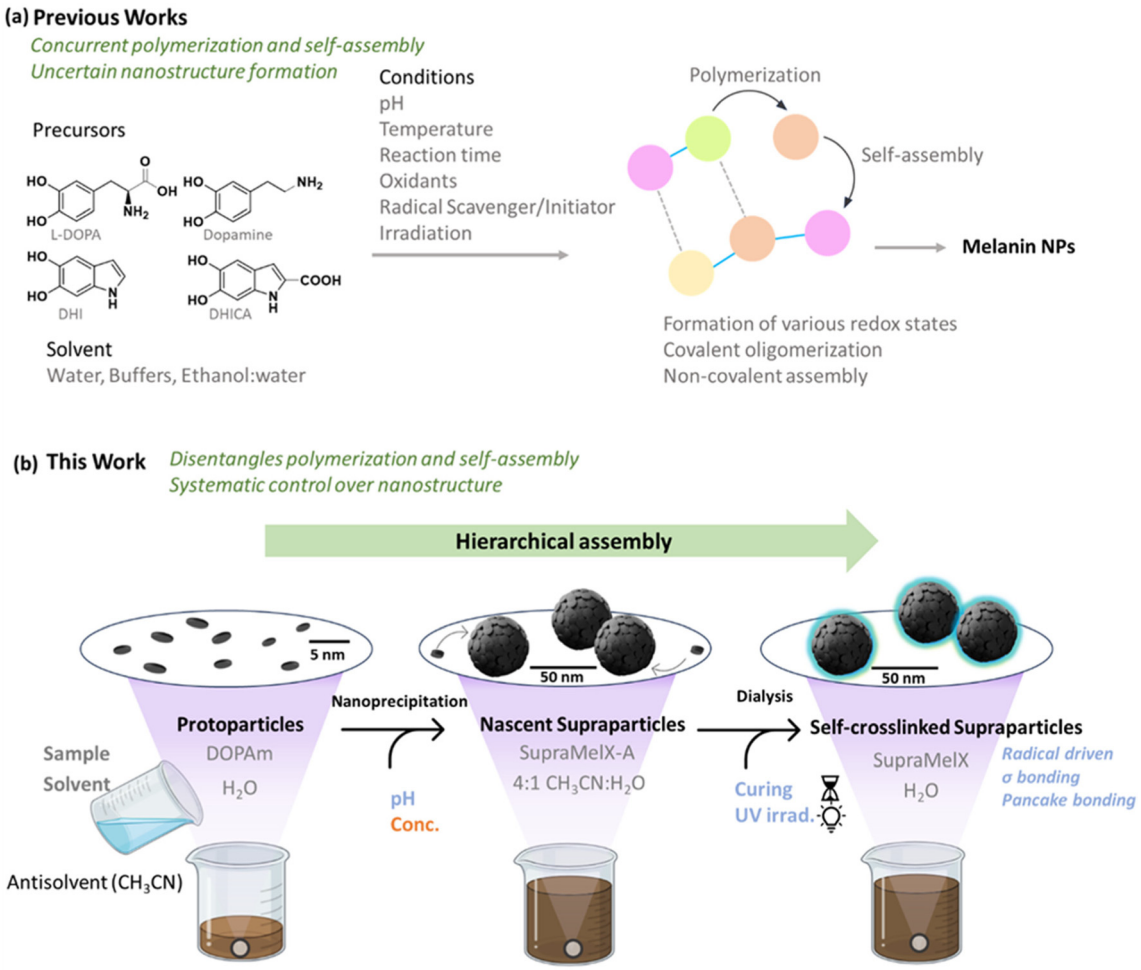

Fig. 1 (a) Previous approaches to control melanin nanostructure using different monomeric precursors and solvents under various reaction conditions. Different colored spheres represent the diversity of intermediate structures and redox states, with nanostructure formation occurring by concurrent polymerization and self-assembly. Covalent bonds are shown as blue lines, and non-covalent interactions as gray dashed lines. (b) Mimicking hierarchical assembly using nanoprecipitation. The schematic illustrates the aggregation of protoparticles of DOPAm into supraparticles of controlled size. Parameters influencing supraparticle size are shown in orange text, while factors affecting particle stability after the removal of acetonitrile are shown in blue. Covalent crosslinks that increase the stability of the final supraparticles are denoted by blue shading. The resulting supraparticles are denoted SupraMel*X*, where *X* is the concentration in mg mL^{-1} of the protoparticle dispersion used for nanoprecipitation. The suffix-A in SupraMel*X*-A indicates an acetonitrile-rich solvent.

to generate structural colors.[25,26] This work demonstrates excellent control of optical properties arising from the spatial arrangement of melanin nanoparticles on micrometer length scales, but control over the intrinsic nanoscale hierarchical structures present within melanin nanoparticles is highly desirable.

Here, we show that the classic synthesis of DOPAm yields ultrasmall (few nm), disc-shaped protoparticles that can be assembled *via* nanoprecipitation into spherical and monodisperse supraparticles 30–100 nm in diameter with excellent size control (Fig. 1b). Nanoprecipitation, a common method for fabricating nanoparticles from polymers, proteins, or small molecules, involves introducing a miscible antisolvent to induce controlled aggregation.[27] The nascent supraparticles are stable to removal of the antisolvent through dialysis. We show that stability correlates with factors that promote free radicals in the particles, suggesting that the aggregated particles are stabilized by radical-driven self-crosslinking reactions. Nanoprecipitation offers a robust method to systematically and reproducibly control melanin nanostructures using the same interactions thought to give rise to the various levels of hierarchical structure in natural melanins.

By pinpointing several factors that influence nanoprecipitation-driven assembly, we achieve nanostructuring in the melanin supraparticles on similar length scales (30–100 nm) as in natural melanin pigments.[28–32] This suggests that self-assembly events taking place during nanoprecipitation may mimic ones that occur during biosynthesis. The ability to controllably achieve sizes similar to ones found in natural melanin particles demonstrates the suitability of melanin supraparticles for various applications, including biomedical applications,[33–35] as well as functional films with antioxidant,[36–38] mechanical,[36,38,39] UV-protecting,[36–39] and conducting properties.[40–42]

Materials and methods

DOPA melanin synthesis

Our synthesis closely follows the classic procedure used to prepare DOPAm in which O_2(g) in air is used to autoxidatively polymerize L-DOPA in alkaline aqueous solution.[43–46] 1 g of L-DOPA (Sigma Aldrich, ≥98%) was added to 200 mL of ultrapure water in a round bottom flask. The pH of the solution was adjusted to 9.5 by adding 1 mL of ammonium hydroxide (Sigma Aldrich, 28–30 wt%) under stirring. Air was continuously bubbled through the reaction mixture, which was stirred continuously for 3 days. The pH was then lowered to 2 by adding a small quantity of 1 M HCl, causing immediate flocculation. The DOPAm was isolated by centrifugation at 10 000*g* for 10 min, and the resulting pellet was washed twice by adding 5 mL of ultrapure water, followed by centrifugation, and removal of the supernatant. Finally, the pellet was dried under flowing N_2(g) for 18 hours, yielding 340 mg of DOPAm (mass yield of 34%).

DOPAm supraparticle size control

A 5 mg mL^{-1} stock solution of DOPAm in ultrapure water was prepared by adjusting the pH to 8 using 1 M NaOH and stirring for 2 h to aid dispersal of the DOPAm powder. The pH of the dispersion after 2 h was approximately 5. After adjusting the pH to 7 by adding a minute volume of 1 M NaOH, the stock solution was diluted with water to prepare 0.5, 1, 2, 3, 4, and 5 mg mL^{-1} dispersions (see Scheme S2). Supraparticles of varying sizes were obtained by adding 4 mL acetonitrile to 1 mL each aqueous dispersion of DOPAm, yielding stable dispersions in 80% v/v acetonitrile with 20% of the original mass concentration. DOPAm supraparticles thus formed remain dispersed in the 4 : 1 acetonitrile : water mixture, which was used for further characterization and isolation. Unless specified for aging studies, both DLS measurements and AFM sample preparation were performed within 1 h of preparing the supraparticles.

Transferring the supraparticles to water

To obtain aqueous dispersions of the supraparticles, a 1 mL aliquot was withdrawn from each SupraMel-A sample in acetonitrile : water and dialyzed against 1 L ultrapure water using a regenerated cellulose dialysis membrane with a 6–8 kDa molecular weight cutoff (MWCO) (Spectra/Por™, 132660T, Repligen) for 24 h (Scheme S3). The solvent moves freely through the dialysis membrane pores, but even the smallest supraparticles are retained in the membrane, so the mass concentration does not change significantly with dialysis. To evaluate pH-dependent stability, a 2 mg mL^{-1} dispersion of DOPAm was adjusted to pH 5, 7, 8, and 10 using 1 M NaOH before adding acetonitrile (Scheme S3a). The resulting acetonitrile : water dispersions were aged for up to 2 days, with aliquots collected and dialyzed every 24 hours. To test the effect of photoirradiation, 1 mL of the SupraMel2 dispersion in acetonitrile : water was irradiated with 372 nm LED for 1.5 h, prior to dialysis. To test stability of the dialyzed supraparticles, the dispersions were aged for a week at room temperature in the dark, sonicated in an ultrasonic bath for up to 10 min, and refluxed for 24 h at 80 °C.

DLS measurements

DLS measurements were performed using a Malvern Panalytical Zetasizer Pro instrument equipped with a He–Ne laser (633 nm) used at a fixed scattering angle of 173°. The as-synthesized supraparticle samples (SupraMel0.5-5) in 4 : 1 (v/v) acetonitrile : water were diluted to a concentration of 0.1 mg mL^{-1} (0.4 absorbance at 633 nm) by adding 80% acetonitrile : water (v/v). The viscosities and refractive indices of 80% v/v acetonitrile dispersion were estimated using the Arrhenius mixing rule and Arago-Biot model, respectively (see SI section S1 for details). The aqueous supraparticle dispersions obtained following dialysis were diluted with water to a concentration of 0.1 mg mL^{-1}. Measurements were conducted using 1 mL aliquots in a 1 cm path-length fused silica cuvette. Data acquisition and analysis were carried out using Malvern

Zetasizer Nano software. For each sample, three consecutive measurements were performed with an acquisition time of 20 s. See SI section S3 for more details on DLS measurements and data processing.

AFM measurements

AFM images were acquired using a Bruker Dimension Icon AFM instrument operated in ScanAsyst™ mode, an off-resonance tapping mode with automatic parameter adjustment. 1 μm × 1 μm images were obtained at 512 samples per line, 0.99 Hz scan rate, and a resolution of 512 × 512 pixels. Measurements were done under ambient conditions using ScanAsyst-Air tips (nominal radius 2 nm, 45–95 kHz, and 0.2–0.8 N m^{-1}) from Bruker. The samples were prepared by dropping 50 μL of the dispersion of interest on freshly cleaved mica followed by drying under nitrogen for 30 minutes. Dispersions for AFM measurements were obtained by diluting a volume of a freshly prepared stock solution to a concentration of 30 μg mL^{-1}. Stock solutions of supraparticles in acetonitrile : water were diluted using acetonitrile, while aqueous dispersions of dialyzed supraparticles were diluted using water. The 5, 10, and 30 μg mL^{-1} dispersions of DOPAm were prepared by diluting a pH 10 stock solution of 2 mg mL^{-1} in water. The large volume of water added caused the pH to drop to ~7. The acquired images were analyzed using NanoScope Analysis 3.00 software (see SI section S4).

Results and discussion

In our approach, nanoprecipitation is used to controllably aggregate melanin nanoparticles into spherical supraparticles (Fig. 1b). The initial melanin nanoparticles were prepared through the spontaneous oxidative polymerization of L-DOPA in alkaline aqueous solution, followed by isolation and drying to produce the powdered DOPA melanin (DOPAm) as described in Materials and Methods. Although the synthetic procedure for producing DOPAm has been widely used for decades, there is still uncertainty about the structures present in aqueous dispersions of DOPAm. For this reason, the next section reports a thorough characterization using atomic force microscopy (AFM) of the initial DOPAm nanoparticles, which are the starting material for our nanoprecipitation experiments. Later sections describe the nanoprecipitation protocol for forming melanin supraparticles and summarize factors that influence their final size and stability after the nascent supraparticles are transferred to aqueous solvent by dialysis.

AFM and DLS analysis of DOPA melanin structures in aqueous dispersions

AFM was used to characterize the morphologies of the DOPAm particles after they are re-dispersed in water and before adding the antisolvent used for nanoprecipitation. The dried DOPAm powder is very difficult to re-disperse in water even after extended stirring and sonication. However, by raising the pH to 8 with 1 M NaOH and stirring for 2 h, a homogeneous stock dispersion with a DOPAm mass concentration of 5 mg mL^{-1} was obtained. The pH of the stirred solution decreased to ~5 due to the release of acidic protons captured by the acid precipitation used to isolate the DOPAm powder (see Materials and Methods). Next, the pH was raised to 10 by adding a drop of 1 M NaOH. Alkaline pH produces supraparticles that can be more easily transferred to water by dialysis as discussed below. To achieve the very low particle concentrations needed for AFM imaging, aliquots from the pH 10 stock dispersion were diluted with ultrapure water to a final DOPAm concentration of between 5–30 μg mL^{-1} and drop cast onto mica. Dilution caused the pH to drop to approximately 7.

The AFM images reveal particles and irregularly shaped flakes that change dramatically in their lateral dimensions with increasing DOPAm concentration (Fig. 2). At the lowest DOPAm concentration of 5 μg mL^{-1}, very small particles <20 nm in diameter are observed but larger more irregularly shaped particles are also seen. For concentrations of 10 μg mL^{-1} and 30 μg mL^{-1}, irregular islands or flakes are seen that have longest dimensions of up to several hundred nm. Larger and more branched particles are observed for the highest concentration (Fig. 2c). Despite the striking changes in lateral dimensions, the structures in all three AFM images have heights between 0.7 nm and 2 nm (Fig. 2), which are comparable to the heights seen in single- and few-layer graphene oxide (GO) on mica.[47–49] Height histograms for the AFM images in Fig. 2 are nearly the same for all three concentrations after excluding the peak at zero height that is caused by unevenness in the mica substrate (Fig. S1). The average height is approximately 1.3 nm for all three images.

Because the average height is independent of the lateral size and initial DOPAm concentration, we conclude that the larger irregular structures form when the smallest particles (protoparticles) seen in all three images aggregate laterally on the mica, possibly driven by H-bonding between functional groups on their edges. Similar edge-to-edge assembly was observed in AFM images of synthetic tyrosine melanin deposited on Mg^{2+}-doped glass cover slips[50] and melanin films on an SiO_2 substrate.[51] In the latter study, islands 1–2 nm tall were observed on top of much thicker films. These islands, which are similar in appearance to the structures in Fig. 2b and c were seen in films spin coated or drop cast from dimethyl sulfoxide (DMSO) dispersions from various melanins, including DOPAm.[51] Our study supports these earlier observations and draws attention to the great proclivity of DOPAm for in-plane growth both on inorganic substrates as well as on itself. The remarkable ability to form smooth conformal coatings has been noted previously for PDA melanin.[52]

We chose the AFM image in Fig. 2a for additional analysis of the lateral particle dimensions. A height threshold was used to identify particles, which are colored cyan against a black background in Fig. S1d. Next, the diameter of a circle having the equivalent area of each contiguous group of cyan pixels was calculated and a histogram of particle diameters was constructed (Fig. S2). The most probable diameter is ~12 nm but particles with equivalent diameters as small as 5 nm and as

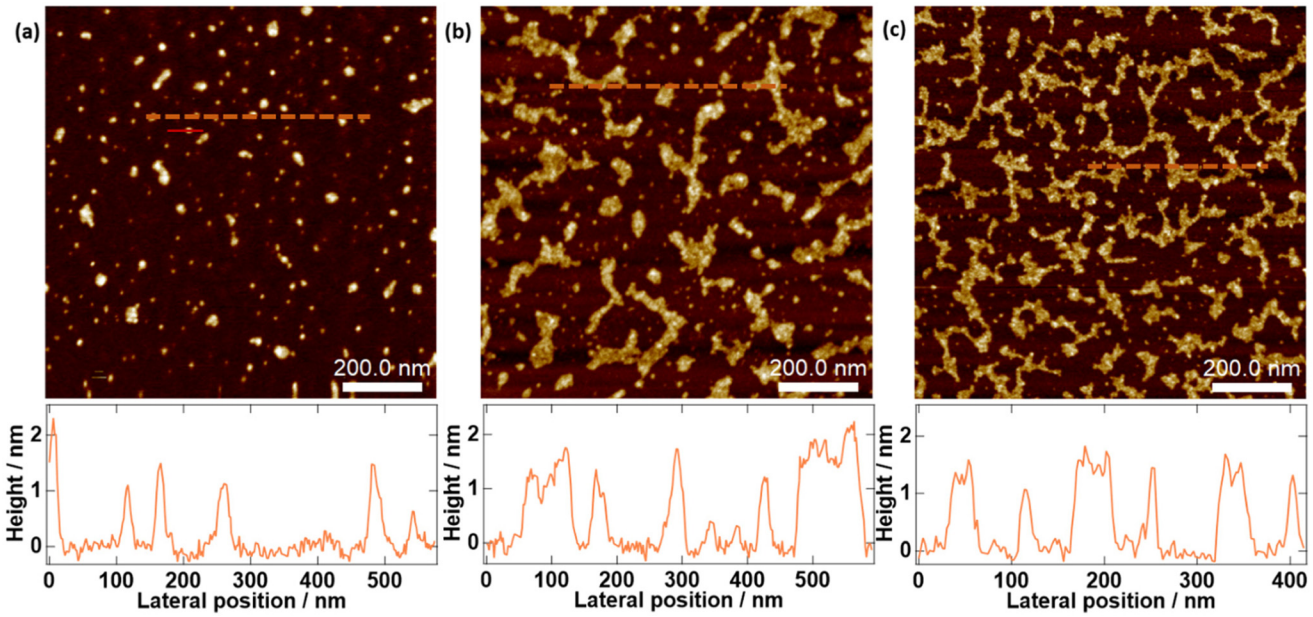

Fig. 2 Morphology of the DOPAm particles prior to nanoprecipitation. AFM images of DOPAm drop cast from (a) 5 μg mL^{-1} (b) 10 μg mL^{-1} and (c) 30 μg mL^{-1} aqueous dispersions. Height profiles along the orange dashed lines (moving from left to right) are shown below each image. The height profile along the red line in panel a is shown in Fig. 3d.

large as 50 nm are observed. The lateral size of the discs agrees well with the features reported for tyrosine melanin (6–30 nm) by Gallas *et al.* using AFM.[50]

The larger structures in Fig. 2a are aggregates of the smallest particles, which assemble in edge-to-edge fashion, possibly through hydrogen bonding interactions between functional groups at their edges. We propose that these two-dimensional aggregates form from the ultrasmall, dot-like particles that are visible in each of the AFM images in Fig. 2 alongside the larger structures. After correcting for convolution broadening due to the finite size of the AFM tip (see SI for details), we estimate that the smallest particles in Fig. 2 have diameters of between 2 and 6 nm.

The DOPAm stock dispersion and the dispersions used to synthesize melanin supraparticles (see next section) have concentrations hundreds of times higher than the dilute samples used in the AFM imaging experiments. To address the nature of the structures present in the higher concentration dispersions, DLS measurements were performed. Low mean DLS count rates of $<10^5$ s^{-1} are observed for aqueous DOPAm dispersions with concentrations between 0.1 and 3.0 mg mL^{-1} (Table S1). These count rates are 1–2 orders of magnitude lower than the observed count rates for dispersions containing spherical nanoparticles with *Z*-average sizes of between 30 and 90 nm (Table S2).

DLS measures the hydrodynamic diameter, which is the size of a sphere that undergoes Brownian diffusion with the same translational diffusion coefficient as the particle. However, nanosheets with a longest dimension of ≥100 nm diffuse much more slowly than spheres of equivalent volume.[53] Lotya *et al.*[53] obtained an empirical equation relating hydrodynamic size measured by DLS to the length of nanosheets of graphene, MoS_2 and WS_2 measured by TEM. Using their relation, a nanosheet with a diameter of 10 nm should diffuse like a spherical particle with a hydrodynamic diameter of 54 nm. However, a particle of this size would produce a DLS count rate at least 50 times higher than the rates we observe for even the most concentrated DOPAm dispersions studied (compare Tables S1 and S2). This result and the finding that the DLS count rates for DOPAm protoparticles do not increase significantly with concentration and are only marginally larger than rates observed for neat water (Table S1) indicate that DOPAm aqueous dispersions with concentrations as high as several mg mL^{-1} do not contain aggregated structures like the ones seen in Fig. 2. Instead, these structures must form during deposition as the solvent evaporates. The particles form extended two-dimensional structures when deposited on mica, which maintain a constant height of 1.3 nm independent of the concentration of the dispersion used for deposition. The average height of 1.3 nm seen here agrees well with heights observed for synthetic melanin particles deposited from methanol[50] and DMSO.[51] The fact that the same height is seen in these diverse experiments suggests that the few-layer stacks seen by AFM do not form at the time of deposition but are already present in the polar solvent dispersions.

The combined AFM and DLS results provide evidence that aqueous dispersions of DOPAm contain copious quantities of small nanosheets a few nm in diameter and between 1.0 and 1.5 nm thick that resemble few-layer stacks of graphene or GO. These dimensions agree very well with ones reported for synthetic and natural melanins using complementary characterization techniques.[50,54–56] For instance, Littrell *et al.*[56] reported

pancake-like particles with an average diameter of 4.6 nm and a thickness of 1.2 nm in aqueous dispersions of tyrosine melanin using small-angle X-ray Scattering (SAXS). In another study, Watt *et al.*[57] identified 2–10 nm curved, plate-like structures in both DOPAm and natural sepia melanin, using high-resolution transmission electron microscopy. Similarly, Strube *et al.*[58] observed 6–10 nm DOPAm particles formed *via* enzyme-mediated synthesis using scanning electron microscopy (SEM). Given that our DOPAm particles can be assembled into larger particles, as shown in the following sections, we adopt the excellent terminology of Strube and co-workers[58] and refer to them as *protoparticles*.

Not all DOPAm samples contain ultrasmall protoparticles. The final size and morphology of melanin particles can differ greatly, depending on synthesis and processing conditions, even when prepared from the same precursor.[1] For example, much larger DOPAm particles (100 nm) have been synthesized using $KMnO_4$ as the oxidant.[10] While it is difficult to disentangle covalent bond formation from non-covalent aggregation, studies on PDA melanin have shown that increasing the rate of polymerization of the precursor results in smaller particles.[14–16] The few-layer protoparticles observed here may be due to our highly oxidizing synthesis conditions (pH 9.5, bubbled air) that promote the rapid oligomerization of L-DOPA. Previously, Chen *et al.*[16] reported <1 nm particles for DOPAm synthesized at pH 10.7 compared to ~20 nm particles when the synthesis was carried out under less oxidizing conditions at pH 8.4.[16]

In nature, eumelanin is synthesized through the enzymatic oxidation of tyrosine by tyrosinase. The enzyme primarily participates in the early steps, hydroxylating tyrosine to L-DOPA and subsequently oxidizing L-DOPA.[59] Beyond these initial reactions, the conversion into eumelanin proceeds largely through spontaneous oxidation and polymerization, making the overall pathway only partially enzyme-controlled.[60] The alkaline and oxidative conditions employed in our synthesis play a comparable role by initiating spontaneous oxidative polymerization of the L-DOPA precursor.[44] While natural melanin forms within a protein-bound environment that can template or constrain nanostructure formation, these scaffolds are not present when synthetic melanins are prepared. Nonetheless, previous studies have shown that hierarchical ordering can still emerge in the absence of proteins—suggesting that such organization is an intrinsic property of melanin assembly.[57,58,61]

Synthesizing size-controlled melanin supraparticles by nanoprecipitation

Inspired by the hierarchical organization observed in natural melanin granules, we explored whether the protoparticles of DOPAm can be assembled into higher-order architectures by modulating interparticle interactions using an antisolvent. Nanoprecipitation is typically used to form nanoparticles from molecular or polymeric precursors and not to assemble pre-existing nanoparticles into supraparticles. However, there are examples where antisolvent addition has been used to assemble small particles present in disordered carbon-based systems.[62,63] Carbon dot suprastructures can be induced through solvothermal treatment,[64] the presence of particular cations,[65] or co-assembly with small molecules or polymers.[66,67] Sarkar *et al.*[62] demonstrated antisolvent-driven assembly by aggregating carbon dots functionalized with amphiphilic surface groups in DMSO into various morphologies using water as the antisolvent. Nanoprecipitation has also been used to form nanoparticles from chemically modified lignin in an organic solvent.[63] Upon adding water, hydrophobic interactions among the aromatic and chemically modified functional groups of lignin drive nanoparticle assembly.

The surface of melanin nanoparticles is rich in functional groups such as hydroxyls, semiquinones, and carboxylic acids. Their deprotonated forms contribute to colloidal stability by generating surface charges. According to a hierarchical model, smaller melanin subunits should contain the same functional groups. Manipulating their charges should thus alter their self-assembly into higher-order structures. Because deprotonation is strongly inhibited in an organic solvent compared to water, we hypothesized that adding an organic solvent to oligomeric melanin protoparticles can manipulate Coulombic interactions between charged DOPAm protoparticles, causing their aggregation into supraparticles.

This hypothesis was tested by adding acetonitrile to a 2 mg mL^{-1} (pH 10) aqueous dispersion of the protoparticles (Scheme S1). After adding acetonitrile, DLS measurement of the acetonitrile : water dispersion diluted to a concentration of 0.1 mg mL^{-1} yielded a derived mean count rate of 1.46×10^6 s^{-1}, a value 20× higher than the one recorded for an aqueous dispersion of protoparticles with the same mass concentration (Table S1). The higher count rate is consistent with the aggregation of protoparticles into larger structures, which we refer to as melanin supraparticles (SupraMel). As indicated in Fig. 1b, we refer to melanin supraparticles dispersed in acetonitrile : water mixed solvents as SupraMel-A, and we drop the suffix-A for supraparticles that have been transferred to water by dialysis (next section).

A uniform size distribution with *Z*-average size of 49 nm was obtained from the DLS measurements (Fig. 3a). As a result of the larger particle size, light scattering from a green laser pointer beam directed through the SupraMel-A sample is easily visible by eye, whereas minimal scattering is seen from a DOPAm aqueous dispersion prior to nanoprecipitation (Fig. 3a inset). The absence of light scattering from the DOPAm sample is consistent with the presence of ultrasmall, well-dispersed protoparticles.

The SupraMel-A particles in the acetonitrile : water mixed solvent were diluted to a concentration of 30 μg mL^{-1} by adding additional acetonitrile followed by drop casting onto a freshly cleaved mica substrate for AFM characterization. The AFM image (Fig. 3b) reveals uniform spherical particles with an average size of 55 nm (Fig. S3) in excellent agreement with the average size determined by DLS (49 nm). Height profiles show that the supraparticles are spherical and vastly larger

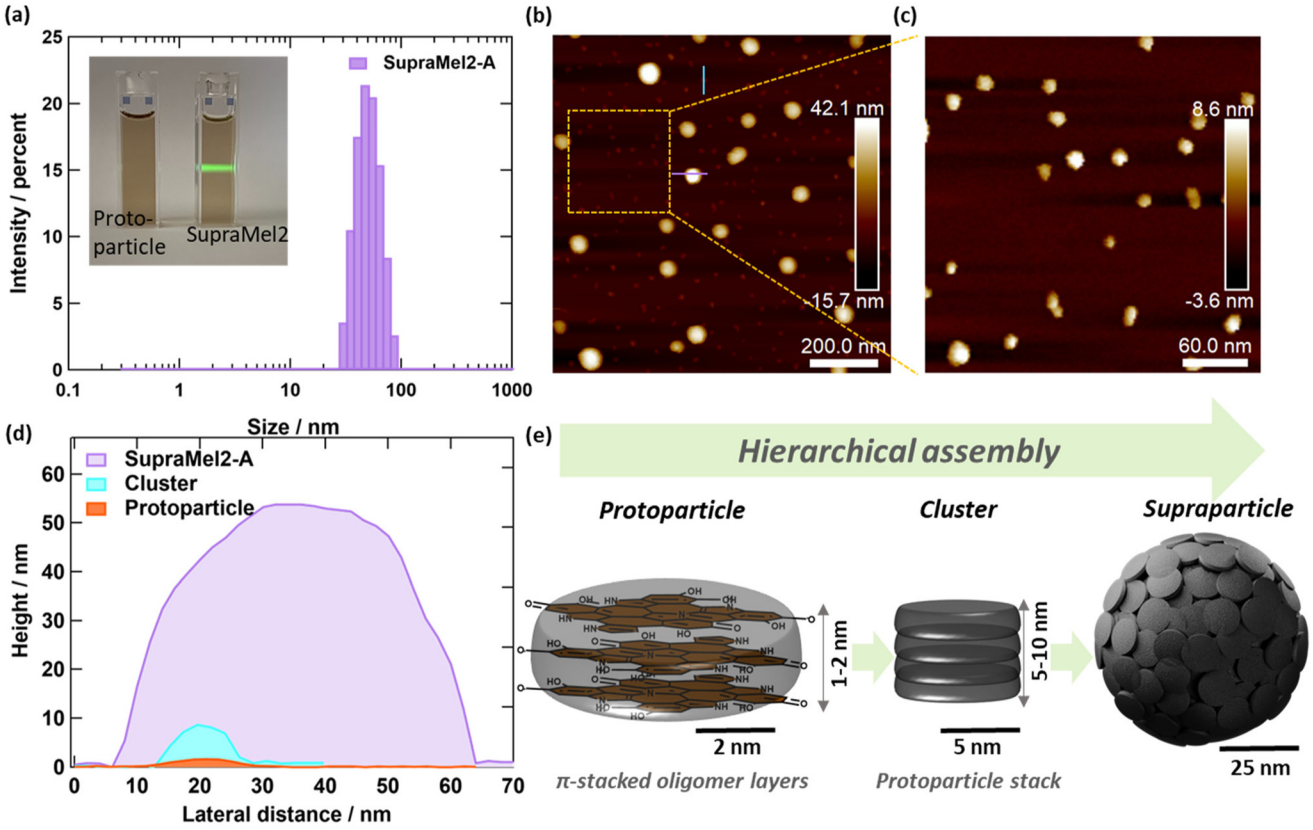

Fig. 3 (a) Intensity-weighted size distribution from DLS measurement of supraparticles with *Z*-average size of 49 nm prepared from an initial pH 10, 2 mg mL^{-1} DOPAm aqueous dispersion. Photographs in the inset compare the light scattering from a green laser pointer for the DOPAm protoparticles in water with the supraparticles in 80% v/v acetonitrile : water. (b) AFM image of the supraparticles in 80% v/v acetonitrile : water revealing uniform spherical particles. (c) Zoomed-in image of the region marked by the yellow dashed square in Fig. 3b, showing smaller clusters. (d) Height profiles of a supraparticle, a cluster and a protoparticle taken along the purple and cyan lines in b, and the red line in Fig. 2a, respectively. (e) Schematic representation of the proposed nanoprecipitation-driven hierarchical assembly.

than protoparticles (Fig. 3d). Considering that disc-shaped protoparticles ~2 nm in diameter and 1.3 nm in height have a volume of ~4 nm^3, a spherical supraparticle with a diameter of 50 nm contains thousands of aggregated protoparticles.

The size and morphology of particles produced by nanoprecipitation have been tuned in previous studies by varying the solvent composition,[68,69] adding surfactants,[51,52,70,71] and by tuning the concentration of the precursor[72,73] or mixing conditions.[71,72] We discovered that the size of the supraparticles depends sensitively on the concentration of the protoparticles in the aqueous dispersion prior to adding acetonitrile (Scheme S2). The SupraMel-A particles can be tuned in size from 30 nm to 100 nm by varying the concentration of protoparticles in the pH 7 dispersion from 1–5 mg mL^{-1} (Fig. 4). Supraparticles formed from different initial DOPAm concentrations are referred to as SupraMel1-5, with the number indicating the concentration in mg mL^{-1} prior to adding acetonitrile. The polydispersity index (PDI) for all SupraMel-A samples is <0.15, indicating uniform particles (Table S2). The AFM images of SupraMel1-A and 3-A (Fig. 4c and d) are consistent with the DLS size distributions (Fig. 4f). The height distributions of the supraparticles are given in Fig. S4.

When the DOPAm concentration is greater than 5 mg mL^{-1}, adding acetonitrile causes flocculation of the DOPAm protoparticles. Nanoprecipitating with a high precursor concentration favors diffusion-controlled aggregation.[74] We propose that supraparticles rapidly coalesce into macrostructures that flocculate when the initial concentration exceeds 5 mg mL^{-1}. For an initial DOPAm concentration of 0.5 mg mL^{-1}, the intensity-weighted DLS size distribution becomes bimodal with 100–200 nm aggregates seen alongside smaller ones <30 nm in size (Fig. S5).

Careful inspection of the AFM images of the SupraMel-A samples in Fig. 3 and 4 reveals a second class of much smaller particles. They appear faint due to their smaller heights, but they are easily recognized with the rescaled colormap in Fig. 3c or by applying a height threshold to the AFM images (Fig. S3b and S4b, d). For the SupraMel2-A sample In Fig. 3c, the smaller particles measure 11 ± 3 nm laterally on average and have an average height of 7 ± 2 nm. This suggests that the smaller particles, which we refer to as clusters, contain 5–6 layers of stacked protoparticles. The clusters are intermediate in size between proto- and supraparticles as shown by a comparison of the AFM height profiles of selected particles

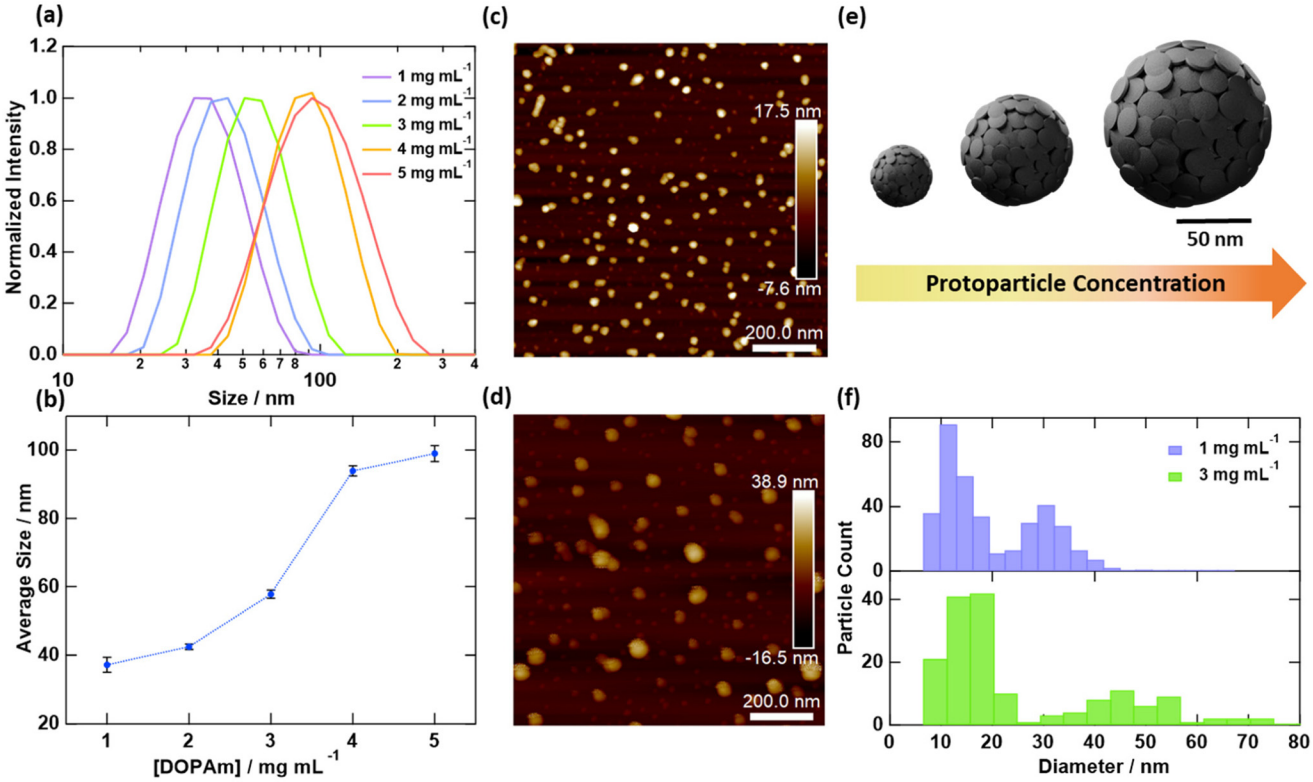

Fig. 4 Size control of supraparticles in aqueous acetonitrile. (a) Normalized intensity distribution of different sized supraparticles prepared by varying the concentration of the initial pH 7 protoparticle dispersion immediately before nanoprecipitation. (b) Average size of supraparticles prepared from different initial protoparticle concentrations. AFM images of supraparticles prepared from (c) 1 mg mL^{-1} and (d) 3 mg mL^{-1} DOPAm dispersions at pH 7. (e) Schematic representation of tuning size of the supraparticles by varying the initial concentration of protoparticles. (f) Diameter distribution of the particles in panels c and d.

(Fig. 3d). However, because they account for <1% by volume of the total material detected in the AFM image, they do not contribute significantly to the DLS measurements.

We propose that the clusters are intermediate states in the hierarchical assembly of the supraparticles (Fig. 3e). Similar 10–30 nm substructures have been previously seen on 100–200 nm *Sepia* melanin particles.[75] Similar size clusters have also been observed to be intermediates that aggregate to form 200–400 nm sized DOPAm particles by Büngeler *et al.*[61] The absence of 1–2 nm sized protoparticles in the AFM images of the supraparticles suggests that all protoparticles are aggregated into clusters upon adding acetonitrile. Understanding the growth kinetics lies outside the scope of this study, but these preliminary findings suggest that supraparticles grow by aggregation of the intermediate clusters. The increase in size of SupraMel-A particles over the course of 72 h is shown in Fig. S6. Taken together, these observations indicate that eumelanin self-assembly proceeds through multiple steps involving persistent intermediate structures whose morphologies are consistent with those seen in natural, hierarchically structured eumelanin.[57,75] While the present data do not resolve whether the intermediate structures are preserved within the final supraparticles or undergo reorganization during assembly, they underscore eumelanin's intrinsic propensity to assemble across multiple length scales.

Recently, Mavridi-Printezi *et al.*[11] reported the formation of two distinct populations during the synthesis of melanin nanoparticles from dopamine: larger nanoparticles with ~100 nm hydrodynamic radii and molecular mass of 10^6 kDa and a fraction with an average hydrodynamic radius of 2.7 nm and 100 kDa molecular mass that the authors termed the polymer-like fraction. These dual structures are reminiscent of the supraparticles and clusters that we observe here. While Mavridi-Printezi *et al.* did not explicitly investigate whether the smaller polymer-like units are precursors to the nanoparticles, our results suggest that such a hierarchical assembly pathway, progressing from protoparticles to clusters to supraparticles is plausible, supporting the idea that the structural subunits of melanin are interconvertible and dynamic.

Stability of the supraparticles in water

Nanostructures formed by antisolvent addition often disaggregate when the antisolvent is removed, especially when the aggregates are held together solely by non-covalent interactions. For example, protein nanoparticles synthesized by the addition of alcohol are unstable and redissolve when the

fraction of water is increased.[76,77] Crosslinking agents such as glutaraldehyde, which forms covalent bonds between amine groups, are often used to stabilize protein nanoparticles in aqueous conditions.[78,79] Chitosan nanoparticles fabricated through nanoprecipitation are another example, where using a crosslinkers like glutaraldehyde or genipin, a natural crosslinking agent, is necessary for particle stability.[80,81] We therefore explored whether the supraparticles remain intact upon removal of acetonitrile.

To remove acetonitrile, SupraMel-A dispersions in 4 : 1 acetonitrile : water were dialyzed against water using a 6–8 kDa membrane for 24 h (Scheme S3). If dialysis is started too soon after adding acetonitrile to the pH 7 protoparticle dispersion, it is not possible to obtain stable supraparticles in water after dialysis. On the other hand, allowing the supraparticles in 4 : 1 acetonitrile : water solvent to stand or cure for a sufficient time prior to dialysis makes it possible to stably transfer the supraparticles to water. We define the curing time as the elapsed time between the addition of acetonitrile and the start of dialysis. A curing time of 48 h was sufficient to allow SupraMel2-A supraparticles to be successfully transferred to aqueous solvent (Fig. S6). With increased curing time, the SupraMel-A particles increase in size as seen by the open circles in Fig. S6. The SupraMel-A particles gradually increase in size with curing time possibly by exchanging or adding clusters.

We propose that stable supraparticles dispersions are obtained in water only when enough crosslinks can form between the constituent protoparticles and clusters. The protoparticles exist as few-layered structures in aqueous dispersions prior to the addition of acetonitrile. Nanoprecipitation with acetonitrile is proposed to bring these structures near enough to one another to form the covalent bonds needed to prevent them from disaggregating into protoparticles again.

The formation of covalent and covalent-like bonds in supraparticles requires the subunits to adopt geometries conducive to bonding. Slow structural rearrangements within the supraparticle may explain why curing times of ≥48 h are required to successfully transfer the SupraMel particles to water. If the curing time is too short, the autocorrelation function obtained from DLS measurements of the post-dialysis dispersion exhibits elevated intensity at the longer time points and a high PDI (Fig. S7), which is characteristic of a heterogeneous, broad size distribution possibly accompanied by large aggregates that undergo slow sedimentation during the measurement.[82] This behavior is diagnostic of supraparticle assemblies that are not stable in the absence of acetonitrile. We note that although the mean scattered DLS count rates measured for post-dialysis dispersions of unstable particles are initially comparable to ones measured for stable supraparticles (around 10^3 kcps), after 48 h in water post-dialysis, the count rates drop to approximately 100 kcps, approaching the rates observed for the DOPAm protoparticles (Table S1). This suggests that supraparticles that do not cure adequately gradually disassemble back into protoparticles because they lack sufficient crosslinking.

We propose that DOPAm supraparticles are stabilized by self-crosslinking reactions that depend on the availability of stable radicals in the protoparticles and clusters. One of the most distinctive properties of melanin is its stable population of free radicals, which are thought to underlie its antioxidant ability and have been harnessed to drive chemical reactions. For example, free radicals on the surface of PDA have been used to initiate free radical polymerization of polymers.[83]

To test our hypothesis, we used two methods known to increase radicals in melanin. In the first method, the pH of the DOPAm protoparticle dispersion in water was raised before adding acetonitrile (Scheme S3a). EPR studies have shown that the free radical population in synthetic melanin increases as the pH is increased.[84] Consistent with the need to have adequate radicals, dispersions of SupraMel2 prepared at higher initial pH required shorter curing times than those formed at lower pH (Fig. 5a). SupraMel2 prepared at pH 10 are stable immediately upon transfer to water, while those formed at pH 8 require 24 h of curing. Particles prepared at pH 7 stabilize after 48 h, and those at pH 5 fail to form stable dispersions in water even after 72 h.

Intensity-weighted size distributions of SupraMel2 prepared at pH 10 before and after dialysis without any curing are com-

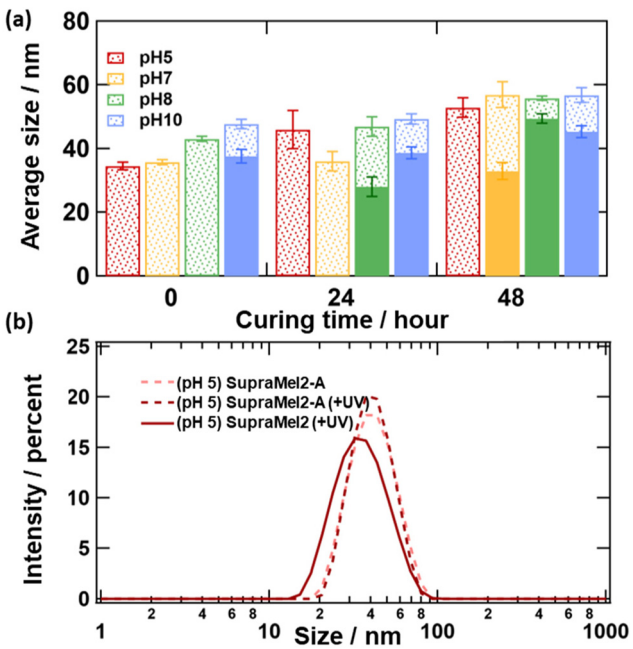

Fig. 5 Factors affecting supraparticle stability. (a) Supraparticle size distribution as a function of the initial pH (5, 7, 8, and 10) of a 2 mg mL^{-1} protoparticle dispersion. Dotted bars show the average particle size for SupraMel2-A in 80% acetonitrile : water before dialysis. Solid bars indicate the average size of the SupraMel2 supraparticles in water after dialysis. (b) DLS intensity-based size distributions for SupraMel2 prepared from an initial pH of 5. The pale dashed line shows the SupraMel-A sample before any irradiation or dialysis in 80% acetonitrile : water. The darker dashed line shows the same sample after 2 h of UV irradiation, as indicated by (+UV). The solid line shows the size distribution after dialysis of the photoirradiated sample, revealing stable supraparticle after photoirradiation.

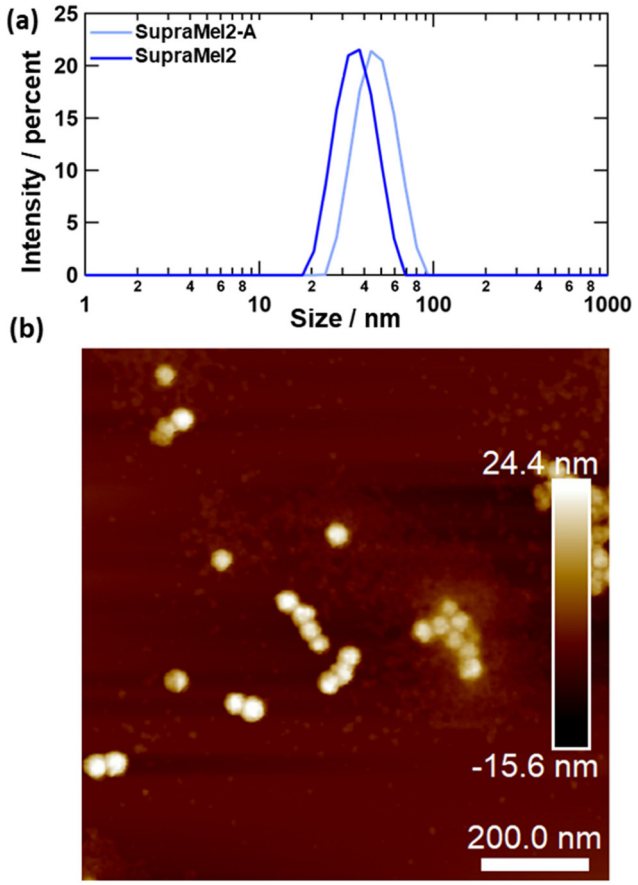

Fig. 6 Characterization of dialyzed supraparticles dispersed in water. (a) Intensity size distribution of SupraMel2 prepared from an initial pH 10 DOPAm dispersion in 80% acetonitrile (SupraMel2-A) and after dialysis into water (SupraMel2). The size distributions indicate that the supraparticles contract by 23% but remain stable after transfer to aqueous media. (b) AFM image of the dialyzed supraparticles deposited on mica, confirming the stability of the supraparticles in the absence of acetonitrile.

pared in Fig. 6a. An AFM image of the dialyzed supraparticles shows uniform spherical particles (Fig. 6b), similar to those observed pre-dialysis (Fig. 3a). The clusters present in the acetonitrile-rich samples (Fig. 3c and 4c, d) are not seen in the AFM images of dialyzed supraparticles (Fig. 6b), probably because they pass through the pores of the dialysis membrane. Notably, the particles formed at pH 10 remain stable in water for at least one week (Fig. S8). We further tested the stability of the supraparticles in water against heating and sonication by refluxing an aqueous dispersion at 80 °C for 24 h and sonicating for up to 10 minutes, respectively. DLS measurements show that the particles are resistant to heating and sonication (Fig. S8).

In a second test for the involvement of radicals in crosslinking, SupraMel2-A particles prepared from an initial pH 5 protoparticle dispersion were irradiated in 4 : 1 acetonitrile : water using a 372 nm LED lamp for 1.5 hours immediately prior to dialysis (Scheme S3b). Photoirradiation is known to increase the concentration of radicals detected by EPR in synthetic and natural melanin.[85,86] Upon dialysis, the irradiated supraparticles remained stable and uniform in water (Fig. 5b), whereas the non-irradiated sample was unstable even after curing for 48 h, according to correlograms obtained from DLS measurements (Fig. S9). The irradiated sample post dialysis shows a *Z*-average size of 34 nm, while a slightly smaller value of 39 nm was measured in 4 : 1 acetonitrile : water before dialysis (Fig. 5b).

The above results argue that melanin's stable radicals contribute to interlayer bonding, and they mirror findings on other disordered carbon materials. For example, Huang *et al.* showed that GO sheets can self-crosslink as they are dehydrated through the formation of inter-sheet ester bonds through condensation reaction between surface carboxylic and OH groups.[87] In melanin, Cheun suggested that functional groups attached to the aromatic rings of eumelanin could form covalent bonds between adjacent layers.[88]

The nature of the bonds that crosslink the supraparticles cannot be assessed at present. Meng and Kaxiras[89] suggested on the basis of DFT calculations that interlayer covalent bonds can form between specific pairs of carbon atoms in small eumelanin oligomers. However, so-called pancake bonding offers an intriguing alternative explanation to the σ-bonding described in ref. 89. Pancake bonding is a covalent-like interaction that leads to multi-center π-bonding between planar moieties with delocalized π radicals.[90] Pancake bonding has been proposed to bond the planar cyclic aromatic hydrocarbons that occur in asphaltenes,[91] and it has recently been discussed for eumelanin.[92] Pancake bonding may be a ubiquitous means of forming insoluble, crosslinked structures in melanin and other carbon-rich nanomaterials.

Conclusions

The hierarchical construction of melanin pigments across nano- and mesoscale dimensions is critical to the multiple functions they provide to natural organisms. The resulting structures shape the redox behavior, radical scavenging capacity, and photophysical properties. However, the spontaneous nature of melanin polymerization leads to considerable structural heterogeneity, obscuring the role of aggregation in establishing these properties. In this study, we applied nanoprecipitation to ~2 nm DOPAm nanosheets or protoparticles to direct the self-assembly of melanin supraparticles (30–100 nm) using an antisolvent. Our approach revealed an intermediate structural motif of 5–6 stacked protoparticles that aggregate into supraparticles by way of small clusters, closely mimicking the hierarchical organization observed in natural melanin. By varying the concentration of the protoparticles, we demonstrated control over the average size of the supraparticles. The resulting supraparticles are stable to antisolvent removal, particularly under conditions that promote free radical formation. These observations suggest that radical-mediated covalent bonding or covalent-like interactions, such

as pancake bonding, contribute to structural stabilization in the synthetic melanin supraparticles and in natural melanins.

Although the assembly of eumelanin oligomers is typically thought to rely on non-covalent interactions such as π–π stacking, hydrogen bonding, or electrostatic interactions,[57,61,93–95] our results strongly suggest that synthetic melanin protoparticles isolated from synthesis can still undergo covalent bonding with each other as they aggregate. Our results challenge the view of melanin as structurally immutable and instead highlight its dynamic nature, which must be considered when processing melanin-like materials. This self-crosslinking behavior, which we propose is common to a broad range of disordered carbon-based nanomaterials warrants further investigation.

We expect that future work will optimize melanin nanoprecipitation to yield even more monodisperse particles that are tunable over a wider range of sizes. Because many of melanin's functional properties depend sensitively on its nanostructure, efforts to control nanoscale morphology are essential for translating melanin-like materials into emerging practical technologies. Applications including drug delivery, imaging, phototherapeutics, and sustainable energy conversion will benefit from reproducible and facile control over melanin nanostructure. By decoupling particle formation from the initial oxidation chemistry, our post-synthetic hierarchical assembly method both provides a powerful tool to systematically study the effects of nano- and mesoscale structuring on eumelanin's properties and enables improved structural control in eumelanin and related materials.

Author contributions

Conceptualization: MM, BK; funding acquisition: BK; investigation: MM, AV, BF; methodology: MM, AV, BF, BK; supervision: BK; writing: MM, BK.

Conflicts of interest

There are no conflicts to declare.

Data availability

Supplementary information (SI): schemes of experimental workflow, additional details on DLS and AFM measurements and analyses, height and particle diameter distributions of AFM images, additional DLS intensity weighted size distributions, and autocorrelation functions. See DOI: https://doi.org/10.1039/d5nr04738b.

Acknowledgements

This work was supported in part by funds from The Ohio Eminent Scholar Program and by the Army Research Office (grant M2504306-TEES). Meera Madhu thanks Dr Yehia Khalifa and Edgar Lopez from the Surface Analysis Laboratory, The Ohio State University for helpful discussions and assistance with the atomic force microscopy measurements.

References

1 M. d'Ischia, K. Wakamatsu, A. Napolitano, S. Briganti, J.-C. Garcia-Borron, D. Kovacs, P. Meredith, A. Pezzella, M. Picardo, T. Sarna, J. D. Simon and S. Ito, Melanins and Melanogenesis: Methods, Standards, Protocols, *Pigm. Cell Melanoma Res.*, 2013, **26**, 616–633.
2 K. A. Motovilov and A. B. Mostert, Melanin: Nature's 4th Bioorganic Polymer, *Soft Matter*, 2024, **20**, 5635–5651.
3 M. d'Ischia, A. Napolitano, A. Pezzella, P. Meredith and M. Buehler, Melanin Biopolymers: Tailoring Chemical Complexity for Materials Design, *Angew. Chem., Int. Ed.*, 2020, **59**, 11196–11205.
4 A. B. Mostert, Melanin, the What, the Why and the How: An Introductory Review for Materials Scientists Interested in Flexible and Versatile Polymers, *Polymers*, 2021, **13**, 1670.
5 L. D'Alba and M. D. Shawkey, Melanosomes: Biogenesis, Properties, and Evolution of an Ancient Organelle, *Physiol. Rev.*, 2019, **99**, 1–19.
6 Bird Coloration, *Mechanisms and Measurements*, ed. G. E. Hill and K. J. McGraw, Series, Harvard University Press, vol. 1, 2006.
7 Q. Li, K.-Q. Gao, Q. Meng, J. A. Clarke, M. D. Shawkey, L. D'Alba, R. Pei, M. Ellison, M. A. Norell and J. Vinther, Reconstruction of Microraptor and the Evolution of Iridescent Plumage, *Science*, 2012, **335**, 1215–1219.
8 K.-Y. Ju, S. Degan, M. C. Fischer, K. C. Zhou, X. Jia, J. Yu and W. S. Warren, Unraveling the Molecular Nature of Melanin Changes in Metastatic Cancer, *J. Biomed. Opt.*, 2019, **24**, 051414.
9 J. B. Nofsinger, E. E. Weinert and J. D. Simon, Establishing Structure–Function Relationships for Eumelanin, *Biopolymers*, 2002, **67**, 302–305.
10 K.-Y. Ju, M. C. Fischer and W. S. Warren, Understanding the Role of Aggregation in the Broad Absorption Bands of Eumelanin, *ACS Nano*, 2018, **12**, 12050–12061.
11 A. Mavridi-Printezi, S. Giordani, A. Menichetti, D. Mordini, A. Zattoni, B. Roda, L. Ferrazzano, P. Reschiglian, V. Marassi and M. Montalti, The Dual Nature of Biomimetic Melanin, *Nanoscale*, 2024, **16**, 299–308.
12 J. B. Nofsinger, Y. Liu and J. D. Simon, Aggregation of Eumelanin Mitigates Photogeneration of Reactive Oxygen Species, *Free Radicals Biol. Med.*, 2002, **32**, 720–730.
13 L. Panzella, G. Gentile, G. D'Errico, N. F. Della Vecchia, M. E. Errico, A. Napolitano, C. Carfagna and M. d'Ischia, Atypical Structural and π-Electron Features of a Melanin Polymer That Lead to Superior Free-Radical-Scavenging Properties, *Angew. Chem., Int. Ed.*, 2013, **52**, 12684–12687.
14 K.-Y. Ju, Y. Lee, S. Lee, S. B. Park and J.-K. Lee, Bioinspired Polymerization of Dopamine to Generate Melanin-Like

Nanoparticles Having an Excellent Free-Radical-Scavenging Property, *Biomacromolecules*, 2011, **12**, 625–632.
15 M. Wu, T. Wang, L. Müller and F. A. Müller, Adjustable Synthesis of Polydopamine Nanospheres and Their Nucleation and Growth, *Colloids Surf., A*, 2020, **603**, 125196.
16 Y. Chen, T. Kendall, P. Yip, A. Davy, J. Sefcik and J. U. Sutter, Influence of Ions and pH on the Formation of Solid- and Liquid-like Melanin, *ACS Omega*, 2020, **5**, 25059–25068.
17 J. E. Lemaster, A. S. Jeevarathinam, A. Kumar, B. Chandrasekar, F. Chen and J. V. Jokerst, Synthesis of Ultrasmall Synthetic Melanin Nanoparticles by UV Irradiation in Acidic and Neutral Conditions, *ACS Appl. Bio Mater.*, 2019, **2**, 4667–4674.
18 X. Wang, Z. Chen, P. Yang, J. Hu, Z. Wang and Y. Li, Size Control Synthesis of Melanin-like Polydopamine Nanoparticles by Tuning Radicals, *Polym. Chem.*, 2019, **10**, 4194–4200.
19 V. Rastogi, S. Melle, O. G. Calderón, A. A. García, M. Marquez and O. D. Velev, Synthesis of Light-Diffracting Assemblies from Microspheres and Nanoparticles in Droplets on a Superhydrophobic Surface, *Adv. Mater.*, 2008, **20**, 4263–4268.
20 W. Liu, M. Kappl, W. Steffen and H.-J. Butt, Controlling Supraparticle Shape and Structure by Tuning Colloidal Interactions, *J. Colloid Interface Sci.*, 2022, **607**, 1661–1670.
21 B. de Nijs, S. Dussi, F. Smallenburg, J. D. Meeldijk, D. J. Groenendijk, L. Filion, A. Imhof, A. van Blaaderen and M. Dijkstra, Entropy-Driven Formation of Large Icosahedral Colloidal Clusters by Spherical Confinement, *Nat. Mater.*, 2015, **14**, 56–60.
22 A. M. Kalsin, M. Fialkowski, M. Paszewski, S. K. Smoukov, K. J. M. Bishop and B. A. Grzybowski, Electrostatic Self-Assembly of Binary Nanoparticle Crystals with a Diamond-Like Lattice, *Science*, 2006, **312**, 420–424.
23 T. Bian, A. Gardin, J. Gemen, L. Houben, C. Perego, B. Lee, N. Elad, Z. Chu, G. M. Pavan and R. Klajn, Electrostatic Co-Assembly of Nanoparticles with Oppositely Charged Small Molecules into Static and Dynamic Superstructures, *Nat. Chem.*, 2021, **13**, 940–949.
24 D. Li, Y. Qu, X. Zhang, W. Zheng, A. L. Rogach and S. Qu, Supra-(Carbon Dots) with Versatile Morphologies and Promising Optical Properties, *Chem. Eng. J.*, 2023, **454**, 140069.
25 M. Xiao, Z. Hu, Z. Wang, Y. Li, A. D. Tormo, N. Le Thomas, B. Wang, N. C. Gianneschi, M. D. Shawkey and A. Dhinojwala, Bioinspired Bright Noniridescent Photonic Melanin Supraballs, *Sci. Adv.*, 2017, **3**, e1701151.
26 Z. Hu, H. Sun, M. P. Thompson, M. Xiao, M. C. Allen, X. Zhou, Q. Z. Ni, Z. Wang, W. Li, M. D. Burkart, D. D. Deheyn, A. Dhinojwala, M. D. Shawkey and N. C. Gianneschi, Structurally Colored Inks from Synthetic Melanin-Based Crosslinked Supraparticles, *ACS Mater. Lett.*, 2021, **3**, 50–55.
27 M. Kuddushi, C. Kanike, B. B. Xu and X. Zhang, Recent Advances in Nanoprecipitation: From Mechanistic Insights to Applications in Nanomaterial Synthesis, *Soft Matter*, 2025, **21**, 2759–2781.
28 E. L. Laden, I. Linden, J. O. Erickson and D. Armen, Electron Microscopic Study of Epidermal Basal Cells and Epidermal Dermal Junction, *J. Invest. Dermatol.*, 1953, **21**, 37–41.
29 M. S. C. Birbeck, E. H. Mercer and N. A. Barnicot, The Structure and Formation of Pigment Granules in Human Hair, *Exp. Cell Res.*, 1956, **10**, 505–514.
30 P. Drochmans, Electron Microscope Studies of Epidermal Melanocytes, and The Fine Structure of Melanin Granules, *J. Biophys. Biochem. Cytol.*, 1960, **8**, 165–180.
31 C. M. R. Clancy and J. D. Simon, Ultrastructural Organization of Eumelanin from Sepia Officinalis Measured by Atomic Force Microscopy, *Biochemistry*, 2001, **40**, 13353–13360.
32 M. Xiao, W. Chen, W. Li, J. Zhao, Y. Hong, Y. Nishiyama, T. Miyoshi, M. D. Shawkey and A. Dhinojwala, Elucidation of the Hierarchical Structure of Natural Eumelanins, *J. R. Soc. Interface*, 2018, **15**, 20180045.
33 J. Park, H. Moon and S. Hong, Recent Advances in Melanin-like Nanomaterials in Biomedical Applications: A Mini Review, *Biomater. Res.*, 2019, **23**, 24.
34 M. Caldas, A. C. Santos, F. Veiga, R. Rebelo, R. L. Reis and V. M. Correlo, Melanin Nanoparticles as a Promising Tool for Biomedical Applications – a Review, *Acta Biomater.*, 2020, **105**, 26–43.
35 A. Mavridi-Printezi, M. Guernelli, A. Menichetti and M. Montalti, Bio-Applications of Multifunctional Melanin Nanoparticles: From Nanomedicine to Nanocosmetics, *Nanomaterials*, 2020, **10**, 2276.
36 S. Shankar, L.-F. Wang and J.-W. Rhim, Effect of Melanin Nanoparticles on the Mechanical, Water Vapor Barrier, and Antioxidant Properties of Gelatin-Based Films for Food Packaging Application, *Food Packag. Shelf Life*, 2019, **21**, 100363.
37 S. Roy and J.-W. Rhim, Preparation of Carrageenan-Based Functional Nanocomposite Films Incorporated with Melanin Nanoparticles, *Colloids Surf., B*, 2019, **176**, 317–324.
38 S. Roy, H. C. Kim, J. W. Kim, L. Zhai, Q. Y. Zhu and J. Kim, Incorporation of Melanin Nanoparticles Improves UV-Shielding, Mechanical and Antioxidant Properties of Cellulose Nanofiber Based Nanocomposite Films, *Mater. Today Commun.*, 2020, **24**, 100984.
39 Ł. Łopusiewicz, F. Jędra and M. Mizielińska, New Poly (Lactic Acid) Active Packaging Composite Films Incorporated with Fungal Melanin, *Polymers*, 2018, **10**, 386.
40 J. P. Bothma, J. de Boor, U. Divakar, P. E. Schwenn and P. Meredith, Device-Quality Electrically Conducting Melanin Thin Films, *Adv. Mater.*, 2008, **20**, 3539–3542.
41 A. Camus, M. Reali, M. Rozel, M. Zhuldybina, F. Soavi and C. Santato, High Conductivity Sepia Melanin Ink Films for

Environmentally Benign Printed Electronics, *Proc. Natl. Acad. Sci. U. S. A.*, 2022, **119**, e2200058119.

42 D. Niyonkuru, A. Camus, M. Reali, Z. Gao, D. M. Shadrack, O. Butyaev, M. Surtchev and C. Santato, A Nanoscale Study of the Structure and Electrical Response of Sepia Eumelanin, *Nanoscale Adv.*, 2023, **5**, 5295–5300.

43 C. C. Felix, J. S. Hyde, T. Sarna and R. C. Sealy, Interactions of Melanin with Metal Ions. Electron Spin Resonance Evidence for Chelate Complexes of Metal Ions with Free Radicals, *J. Am. Chem. Soc.*, 1978, **100**, 3922–3926.

44 L. E. Arnow, The Preparation of Dopa-Melanin, *Science*, 1938, **87**, 308–308.

45 F. Binns, R. F. Chapman, N. C. Robson, G. A. Swan and A. Waggott, Studies Related to the Chemistry of Melanins. Part VIII. The Pyrrole-carboxylic Acids formed by Oxidation or Hydrolysis of Melanins derived from 3,4-Dihydroxyphenethylamine or (±)-3,4-Dihydroxyphenylalanine, *J. Chem. Soc. C*, 1970, 1128–1134.

46 G. Szewczyk, A. Zadlo, M. Sarna, S. Ito, K. Wakamatsu and T. Sarna, Aerobic Photoreactivity of Synthetic Eumelanins and Pheomelanins: Generation of Singlet Oxygen and Superoxide Anion, *Pigm. Cell Melanoma Res.*, 2016, **29**, 669–678.

47 Q. Lai, S. Zhu, X. Luo, M. Zou and S. Huang, Ultraviolet-Visible Spectroscopy of Graphene Oxides, *AIP Adv.*, 2012, **2**, 032146.

48 Y. Chong, C. Ge, G. Fang, X. Tian, X. Ma, T. Wen, W. G. Wamer, C. Chen, Z. Chai and J.-J. Yin, Crossover between Anti- and Pro-Oxidant Activities of Graphene Quantum Dots in the Absence or Presence of Light, *ACS Nano*, 2016, **10**, 8690–8699.

49 J. Park, W. Lee, J. Nam, J. T. Han, C.-J. Choi and J. Y. Hwang, A Study of the Correlation between the Oxidation Degree and Thickness of Graphene Oxides, *Carbon*, 2022, **189**, 579–585.

50 J. M. Gallas, G. W. Zajac, T. Sarna and P. L. Stotter, Structural Differences in Unbleached and Mildly-Bleached Synthetic Tyrosine-Derived Melanins Identified by Scanning Probe Microscopies, *Pigm. Cell Res.*, 2000, **13**, 99–108.

51 J. Wünsche, F. Cicoira, C. F. O. Graeff and C. Santato, Eumelanin Thin Films: Solution-Processing, Growth, and Charge Transport Properties, *J. Mater. Chem. B*, 2013, **1**, 3836–3842.

52 H. Lee, S. M. Dellatore, W. M. Miller and P. B. Messersmith, Mussel-Inspired Surface Chemistry for Multifunctional Coatings, *Science*, 2007, **318**, 426–430.

53 M. Lotya, A. Rakovich, J. F. Donegan and J. N. Coleman, Measuring the Lateral Size of Liquid-Exfoliated Nanosheets with Dynamic Light Scattering, *Nanotechnology*, 2013, **24**, 265703.

54 G. W. Zajac, J. M. Gallas, J. Cheng, M. Eisner, S. C. Moss and A. E. Alvarado-Swaisgood, The Fundamental Unit of Synthetic Melanin: A Verification by Tunneling Microscopy of X-Ray Scattering Results, *Biochim. Biophys. Acta, Gen. Subj.*, 1994, **1199**, 271–278.

55 J. I. N. Cheng, S. C. Moss and M. Eisner, X-Ray, Characterization of Melanins—II, *Pigm. Cell Res.*, 1994, **7**, 263–273.

56 K. C. Littrell, J. M. Gallas, G. W. Zajac and P. Thiyagarajan, Structural Studies of Bleached Melanin by Synchrotron Small-Angle X-Ray Scattering, *Photochem. Photobiol.*, 2003, **77**, 115–120.

57 A. A. R. Watt, J. P. Bothma and P. Meredith, The Supramolecular Structure of Melanin, *Soft Matter*, 2009, **5**, 3754–3760.

58 O. I. Strube, A. Büngeler and W. Bremser, Enzyme-Mediated In Situ Synthesis and Deposition of Nonaggregated Melanin Protoparticles, *Macromol. Mater. Eng.*, 2016, **301**, 801–804.

59 A. B. Lerner and T. B. Fitzpatrick, Biochemistry of Melanin Formation, *Physiol. Rev.*, 1950, **30**, 91–126.

60 M. d'Ischia, A. Napolitano, V. Ball, C.-T. Chen and M. J. Buehler, Polydopamine and Eumelanin: From Structure–Property Relationships to a Unified Tailoring Strategy, *Acc. Chem. Res.*, 2014, **47**, 3541–3550.

61 A. Büngeler, B. Hämisch and O. I. Strube, The Supramolecular Buildup of Eumelanin: Structures, Mechanisms, Controllability, *Int. J. Mol. Sci.*, 2017, **18**, 1901.

62 S. Sarkar, S. Dinda, P. Choudhury and P. K. Das, Self-Assembly of Surface Functionalized Amphiphilic Carbon Dots: Tuning in Morphological Manifestations, *Soft Matter*, 2019, **15**, 2863–2875.

63 Q. Li, H. Zhang, J. Lee and C. Wan, Size-Tailorable Lignin Nanoparticle Synthesis: Effects of Solution Chemistry and DLVO Forces on Amphiphilic Balance of Lignin, *Green Chem.*, 2023, **25**, 9301–9312.

64 J. Wu, J. H. Lei, B. He, C.-X. Deng, Z. Tang and S. Qu, Generating Long-Wavelength Absorption Bands with Enhanced Deep Red Fluorescence and Photothermal Performance in Fused Carbon Dots Aggregates, *Aggregate*, 2021, **2**, e139.

65 Q. Li, B. Chen and B. Xing, Aggregation Kinetics and Self-Assembly Mechanisms of Graphene Quantum Dots in Aqueous Solutions: Cooperative Effects of pH and Electrolytes, *Environ. Sci. Technol.*, 2017, **51**, 1364–1376.

66 Q. Jia, J. Ge, W. Liu, X. Zheng, S. Chen, Y. Wen, H. Zhang and P. Wang, A Magnetofluorescent Carbon Dot Assembly as an Acidic H_2O_2-Driven Oxygenerator to Regulate Tumor Hypoxia for Simultaneous Bimodal Imaging and Enhanced Photodynamic Therapy, *Adv. Mater.*, 2018, **30**, 1706090.

67 N. T. N. Hang, N. Van Canh, N. H. Hoa, P. D. Du, P. H. Le and V. Nguyen, Co-Assembled Hybrid of Carbon Nanodots and Molecular Fluorophores for Efficient Solar-Driven Water Evaporation, *Carbon*, 2022, **199**, 462–468.

68 G. Bovone, L. Cousin, F. Steiner and M. W. Tibbitt, Solvent Controls Nanoparticle Size during Nanoprecipitation by Limiting Block Copolymer Assembly, *Macromolecules*, 2022, **55**, 8040–8048.

69 M. Núñez-Martínez, M. Fernández-Míguez, E. Quiñoá and F. Freire, Size Control of Chiral Nanospheres Obtained via

Nanoprecipitation of Helical Poly(Phenylacetylene)s in the Absence of Surfactants, *Angew. Chem., Int. Ed.*, 2024, **63**, e202403313.

70 S. F. Chin, S. C. Pang and S. H. Tay, Size Controlled Synthesis of Starch Nanoparticles by a Simple Nanoprecipitation Method, *Carbohydr. Polym.*, 2011, **86**, 1817–1819.

71 J. G. J. L. Lebouille, R. Stepanyan, J. J. M. Slot, M. A. Cohen Stuart and R. Tuinier, Nanoprecipitation of Polymers in a Bad Solvent, *Colloids Surf., A*, 2014, **460**, 225–235.

72 W. Huang and C. Zhang, Tuning the Size of Poly(Lactic-Co-Glycolic Acid) (PLGA) Nanoparticles Fabricated by Nanoprecipitation, *Biotechnol. J.*, 2018, **13**, 1700203.

73 K. Tanaka, H. Kuramochi, K. Maeda, Y. Takahashi, M. Osako and G. Suzuki, Size-Controlled Preparation of Polyethylene Nanoplastic Particles by Nanoprecipitation and Insights into the Underlying Mechanisms, *ACS Omega*, 2023, **8**, 14470–14477.

74 E. Lepeltier, C. Bourgaux and P. Couvreur, Nanoprecipitation and the "Ouzo Effect": Application to Drug Delivery Devices, *Adv. Drug Delivery Rev.*, 2014, **71**, 86–97.

75 Y. Liu and J. D. Simon, Isolation and Biophysical Studies of Natural Eumelanins: Applications of Imaging Technologies and Ultrafast Spectroscopy, *Pigm. Cell Res.*, 2003, **16**, 606–618.

76 K. J. Geh, M. Hubert and G. Winter, Optimisation of One-Step Desolvation and Scale-up of Gelatine Nanoparticle Production, *J. Microencapsulation*, 2016, **33**, 595–604.

77 L. C. Nelemans, V. A. Melo, M. Buzgo, E. Bremer and A. Simaite, Antibody Desolvation with Sodium Chloride and Acetonitrile Generates Bioactive Protein Nanoparticles, *PLoS One*, 2024, **19**, e0300416.

78 C. Weber, C. Coester, J. Kreuter and K. Langer, Desolvation Process and Surface Characterisation of Protein Nanoparticles, *Int. J. Pharm.*, 2000, **194**, 91–102.

79 W. Lohcharoenkal, L. Wang, Y. C. Chen and Y. Rojanasakul, Protein Nanoparticles as Drug Delivery Carriers for Cancer Therapy, *BioMed Res. Int.*, 2014, **2014**, 180549.

80 B. R. Riegger, B. Bäurer, A. Mirzayeva, G. E. M. Tovar and M. Bach, A Systematic Approach of Chitosan Nanoparticle Preparation via Emulsion Crosslinking as Potential Adsorbent in Wastewater Treatment, *Carbohydr. Polym.*, 2018, **180**, 46–54.

81 C. Vila-Sanjurjo, L. Hembach, J. Netzer, C. Remuñán-López, A. Vila-Sanjurjo and F. M. Goycoolea, Covalently and Ionically, Dually Crosslinked Chitosan Nanoparticles Block Quorum Sensing and Affect Bacterial Cell Growth on a Cell-Density Dependent Manner, *J. Colloid Interface Sci.*, 2020, **578**, 171–183.

82 F. Caputo, R. Vogel, J. Savage, G. Vella, A. Law, G. Della Camera, G. Hannon, B. Peacock, D. Mehn, J. Ponti, O. Geiss, D. Aubert, A. Prina-Mello and L. Calzolai, Measuring Particle Size Distribution and Mass Concentration of Nanoplastics and Microplastics: Addressing Some Analytical Challenges in the Sub-Micron Size Range, *J. Colloid Interface Sci.*, 2021, **588**, 401–417.

83 C. G. Bailey, M. D. Nothling, L. L. Fillbrook, Y. Vo, J. E. Beves, D. R. McCamey and M. H. Stenzel, Polydopamine as a Visible-Light Photosensitiser for Photoinitiated Polymerization, *Angew. Chem. Int. Ed.*, 2023, **62**, e202301678.

84 T. Sarna, A. Dulęba, W. Korytowski and H. Swartz, Interaction of Melanin with Oxygen, *Arch. Biochem. Biophys.*, 1980, **200**, 140–148.

85 R. J. Sever, F. W. Cope and B. D. Polis, Generation by Visible Light of Labile Free Radicals in the Melanin Granules of the Eye, *Science*, 1962, **137**, 128–129.

86 T. Sarna and R. C. Sealy, Free Radicals from Eumelanins: Quantum Yields and Wavelength Dependence, *Arch. Biochem. Biophys.*, 1984, **232**, 574–578.

87 H. Huang, H. Park and J. Huang, Self-Crosslinking of Graphene Oxide Sheets by Dehydration, *Chem*, 2022, **8**, 2432–2441.

88 W. L. Cheun, The Chemical Structure of Melanin, *Pigm. Cell Res.*, 2004, **17**, 422–423.

89 S. Meng and E. Kaxiras, Theoretical Models of Eumelanin Protomolecules and Their Optical Properties, *Biophys. J.*, 2008, **94**, 2095–2105.

90 M. Kertesz, Pancake Bonding: An Unusual Pi-Stacking Interaction, *Chem. – Eur. J.*, 2019, **25**, 400–416.

91 Y. Zhang, M. Siskin, M. R. Gray, C. C. Walters and R. P. Rodgers, Mechanisms of Asphaltene Aggregation: Puzzles and a New Hypothesis, *Energy Fuels*, 2020, **34**, 9094–9107.

92 P. A. Abramov, O. I. Ivankov, A. B. Mostert and K. A. Motovilov, Signatures of Pancake Bonding in Hydrated Eumelanin, *Phys. Chem. Chem. Phys.*, 2023, **25**, 16212–16216.

93 A. Mavridi-Printezi, A. Menichetti, L. Ferrazzano and M. Montalti, Reversible Supramolecular Noncovalent Self-Assembly Determines the Optical Properties and the Formation of Melanin-like Nanoparticles, *J. Phys. Chem. Lett.*, 2022, **13**, 9829–9833.

94 M. Arzillo, G. Mangiapia, A. Pezzella, R. K. Heenan, A. Radulescu, L. Paduano and M. d'Ischia, Eumelanin Buildup on the Nanoscale: Aggregate Growth/Assembly and Visible Absorption Development in Biomimetic 5,6-Dihydroxyindole Polymerization, *Biomacromolecules*, 2012, **13**, 2379–2390.

95 S. Hong, Y. Wang, S. Y. Park and H. Lee, Progressive Fuzzy Cation-π Assembly of Biological Catecholamines, *Sci. Adv.*, 2018, **4**, eaat7457.

